Topological Analysis of Point Singularities in Stimulus Preference Maps of the Primary Visual Cortex

Author(s): Shigeru Tanaka

Source: *Proceedings: Biological Sciences*, Vol. 261, No. 1360 (Jul. 22, 1995), pp. 81-88
Published by: The Royal Society
Stable URL: http://www.jstor.org/stable/50050

Topological analysis of point singularities in stimulus preference maps of the primary visual cortex

SHIGERU TANAKA

Laboratory for Neural Networks, Frontier Research Program, The Institute of Physical and Chemical Research (RIKEN) 2-1 Hirosawa, Wako, Saitama 351-01, Japan
and Fundamental Research Laboratories, NEC 34 Miyukigaoka, Tsukuba, Ibaraki 305, Japan

SUMMARY

A large population of neurons in the primary visual cortex optimally respond to the orientation and phase of a grating stimulus in luminance. I demonstrate here that the topology of the stimulus space spanned by these parameters is equivalent to that of the Klein bottle, which has a characteristic feature that there is no distinction between the inside and outside of the bottle. The assumption that these stimulus parameters are continuously arranged almost everywhere on the visual cortical surface enables us to map from a loop on the cortical surface to a loop on the Klein bottle. This leads to a systematic categorization of possible point singularities in the arrangements of the optimal orientation and phase in the cortex. Two types of point singularities have been observed in the orientation preference map, according to clockwise or counterclockwise rotation in optimal orientation around the points. The present analysis predicts that each type of orientation centre is subdivided into two types, around which neurons exhibit separately ON-centre and OFF-flank or OFF-centre ON-flank receptive fields. It is also predicted that point singularities about the optimal phase are allowed to exist on the cortical surface. Finally, these predictions are tested by computer simulation based on the author's thermodynamic model for neural network self-organization.

1. INTRODUCTION

Each neuron in the primary visual cortex responds to a luminance grating presented within a specific area of the visual space (receptive field, RF) with a certain orientation (Hubel & Wiesel 1962). Recent experiments have revealed that the optimal orientation continuously changes along the cortical surface to form an orderly map (Bonhoeffer & Grinvald 1991; Blasdel 1992) shown in figure 1. This map is characterized by point singularities, the so-called orientation centres (Bonhoeffer & Grinvald 1991; Blasdel 1992), at which all orientations from 0° to 180° converge in a pinwheel-like structure (indicated by the solid squares in figure 1).

To reproduce overall structures of the orientation preference map, various models have been proposed (von der Malsburg 1973; Linsker 1986; Durbin & Mitchison 1990; Obermayer *et al.* 1990; Miller 1992; Miyashita & Tanaka 1992). In most of these models, the *a priori* existence of optimal stimulus parameters was assumed without discussing how the neural connections are arranged to produce neuronal responses (Durbin & Mitchison 1990; Obermayer *et al.* 1990). In such models, the space spanned by optimal stimulus parameters is given by the direct product of spaces spanned by individual parameters. There is another line of research on the formation of stimulus preference maps, which attempts to reproduce RF profiles of individual cortical cells and cortical arrangements of parameters relevant to the RFs simultaneously through the self-organization of afferent geniculate inputs (Miller 1992; Miyashita & Tanaka 1992). In the latter approach, a basic idea is that optimal stimulus parameters should be extracted from the RF profiles obtained from the self-organization of afferent inputs. That is, the RF is more important than optimal stimulus parameters extracted from the RFs. This idea turns out to be critical when we refer to hidden symmetries of optimal stimulus parameters.

The main objective of this paper is to explain the characteristic features of the orientation preference map by using topological properties of the RFs. I assumed that RFs of some portions of cortical cells can be expressed by the Gabor function, and that the RF changes continuously almost everywhere on the cortical surface with the change in the position of the neurons. Here I focused on the optimal orientation and phase. A hidden symmetry inherent in the stimulus space obtained from an invariant transformation of the RF leads to a topological equivalence between the stimulus space and the Klein bottle (Bredon 1993). By applying the homotopy theory to the stimulus space, topologically possible point singularities are derived. Finally, using computer simulation, it is confirmed that the point singularities are allowed to exist energetically as well as topologically.

Proc. R. Soc. Lond. B (1995) **261**, 81–88
Printed in Great Britain

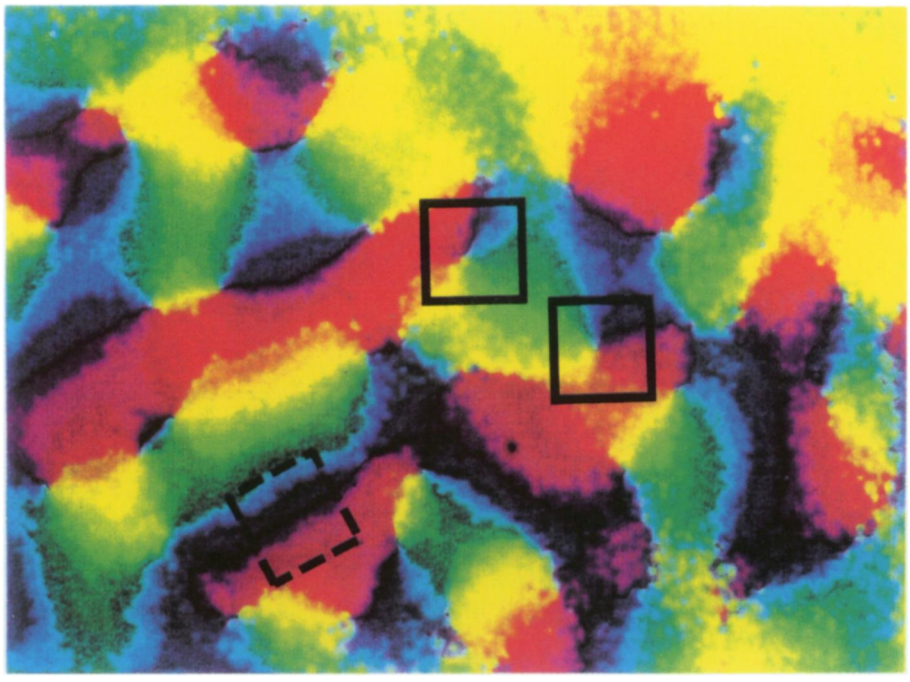

Figure. 1. Observed iso-orientation domains in area 17 of the cat. All of the colours from yellow to orange represent domains of similar orientations from 0° to 180° in which neurons exhibit optimal responses to oriented gratings of luminance presented on the TV monitor set in front of the animal. The picture contains point singularities called orientation centres at which all the colours are organized to converge although the colour changes gradually in other areas. If the orientation changes by 180° when we move along a closed circle on the cortical surface, the circle contains an orientation centre within it, as shown by the solid squares in the picture. Otherwise, it does not contain an orientation centre, as shown by the dotted square. (Courtesy of Professor Amiram Grinvald.)

2. DERIVATION OF THE KLEIN BOTTLE AS THE STIMULUS SPACE

The RFs of simple cells are composed of ON and OFF subfields at which the exposure to light stimuli facilitates and suppresses the neuronal activity, respectively. These subfields are alternately arranged parallel to the optimal orientations of the cells. Therefore, the cell responses are maximal for optimally oriented gratings located at appropriate positions within their RFs. These features of RFs can be expressed by the following Gabor functions of the position vector defined in the visual space: $R(\boldsymbol{x}) = A \exp(-\boldsymbol{x}^2/(2\sigma^2)) \cos(2\pi f \boldsymbol{e}(\theta)\cdot\boldsymbol{x} - \phi)$, where θ and ϕ represent the orientation and phase, and A, σ, f, and $\boldsymbol{e}$ represent the normalization factor of response strength, width of the RF, spatial frequency and unit vector vertical to the orientation θ, respectively. Here, we focus (in particular) on the optimal orientation θ and phase ϕ. The best fit of this function with the RFs is obtained by choosing values of the two parameters within the intervals $0° \leqslant \theta < 180°$ and $0° \leqslant \phi < 360°$ (Daugman 1980; Marcelja 1980), as depicted by the rectangular domain of figure 2*a*. Within this domain, the RF is defined as a single-valued function of θ and ϕ. The white and black ovals in figure 2*a* show the ON and OFF subfields, respectively, in the representative RFs derived from the Gabor function which should occur along the edges of the domain. It is noted that identical configurations of ON and OFF subfields appear along the opposite edges of the domain. ON-centre OFF-flank RFs rotate clockwise along both horizontal edges from 0° to 180° of the orientation. On the other hand, the RF configuration changes in opposite ways along the two vertical edges from 0° to 360° of the phase. Therefore, the configuration of subfields within an RF changes continuously in the direction indicated by the arrows.

The points that represent identical RFs can be pasted together to obtain a closed manifold. The rectangular domain of the stimulus space can be formed into a tube by rolling and pasting together the two identical horizontal edges (see figure 2*b*). This tube has directed circles at the two ends. Next, by twisting the tube and pasting the two identical ends together so that their directions coincide, we obtain the Klein bottle (see figure 2*c*, *d*). Consequently, the horizontal and vertical edges of the rectangular domain are transformed to directed closed paths or loops l and n on the Klein bottle, respectively.

Generally a given manifold can be categorized to an orientable or unorientable one: the coordinate can be uniquely defined over the orientable manifold, whereas a locally defined coordinate is not consistent over the unorientable manifold. The Klein bottle, denoted by K^2, is known as an example of an unorientable manifold, whereas the sphere S^2 and torus T^2 are orientable and divide the three-dimensional space into an inside and an outside. Hence the Klein bottle is characterized by a peculiar feature in that its inside cannot be distinguished from its outside. Note that the Klein bottle does not intersect with itself although it may appear to do so from the illustration (see figure 2*d*). Strictly speaking, the Klein bottle cannot be embedded in the Euclidian space of fewer than four dimensions.

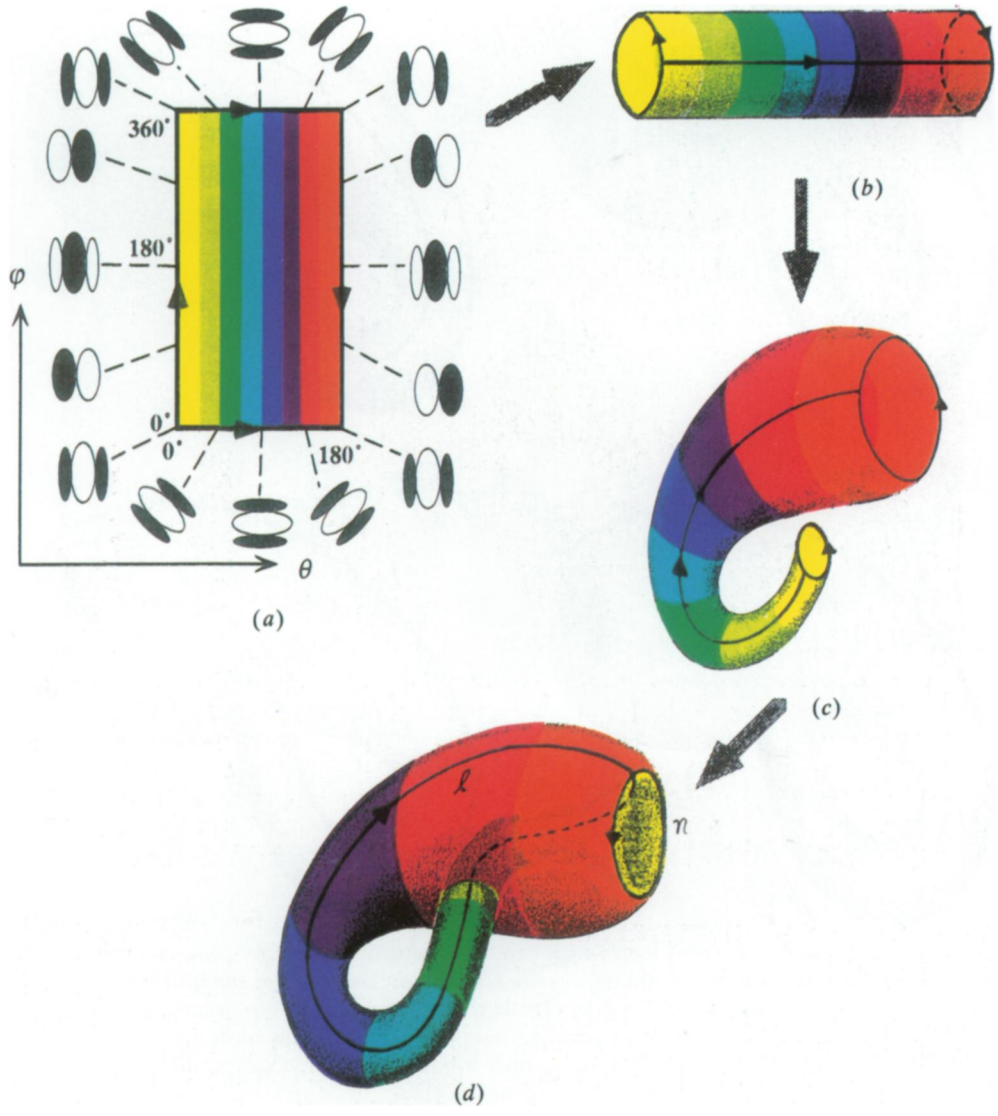

Figure 2. How to construct the Klein bottle from symmetry properties of RF profiles. (*a*) For simple cells in the primary visual cortex, the RF profile can be specified by two major parameters: optimal orientation θ and phase ϕ. We focus in particular on these parameters defined in the rectangular domain: $0° \leqslant \theta < 180°$ and $0° \leqslant \phi < 360°$. Only the RF profiles specified by the representative points along the edges of the domain are illustrated. Each colour represents a group of similarity in optimal orientation. (*b*) Identical RF profiles appear on opposite edges of the rectangular domain, and they change in the same manner in the direction indicated by the arrows. (*c*), (*d*) By pasting the pairs of identical edges together so that their directions coincide, the rectangular domain becomes the Klein bottle. Note that the horizontal and vertical edges of the domain are transformed to loops on the Klein bottle along and around the bottle axis, respectively.

3. CLASSIFICATION OF LOOPS ON THE KLEIN BOTTLE

In the homotopy theory, when a directed loop α in a topological space X is given by continuous deformation of another directed loop β in the same space, these two loops are defined as identical to each other, and are called homotopic in the space X. All loops which are homotopic form a class, i.e. a homotopy class. Although there are an infinite number of loops in a topological space in general, all the possible loops can be categorized into classes in this manner. By introducing the product of loops, the operation of linking loops together into one, the homotopy classes form a group. The associative law is satisfied for the loop product, and homotopic loops corresponding to the unit and inverse exist. This group $\pi_1(X)$ is termed the 1st homotopy group of the space X.

By employing these mathematics, each loop on the Klein bottle can be categorized into a homotopy class. The 1st homotopy group of the Klein bottle $\pi_1(K^2)$ is known to be equivalent to the group $Z \otimes Z_2$, i.e. the direct product of the group of integers, Z, and the group of integers modulo 2, Z_2 (Bredon 1993). The elements of Z represent the winding numbers of a loop along the Klein bottle axis. However, each element of Z_2 represents the presence or absence of a loop around the Klein bottle axis. This indicates that each homotopy class of loops on the Klein bottle can be specified by the combination of integers (p, q) for $p = 0, \pm 1, \pm 2, \ldots$ and $q = 0$ or 1. The sign of p indicates that the direction of the loops is clockwise or

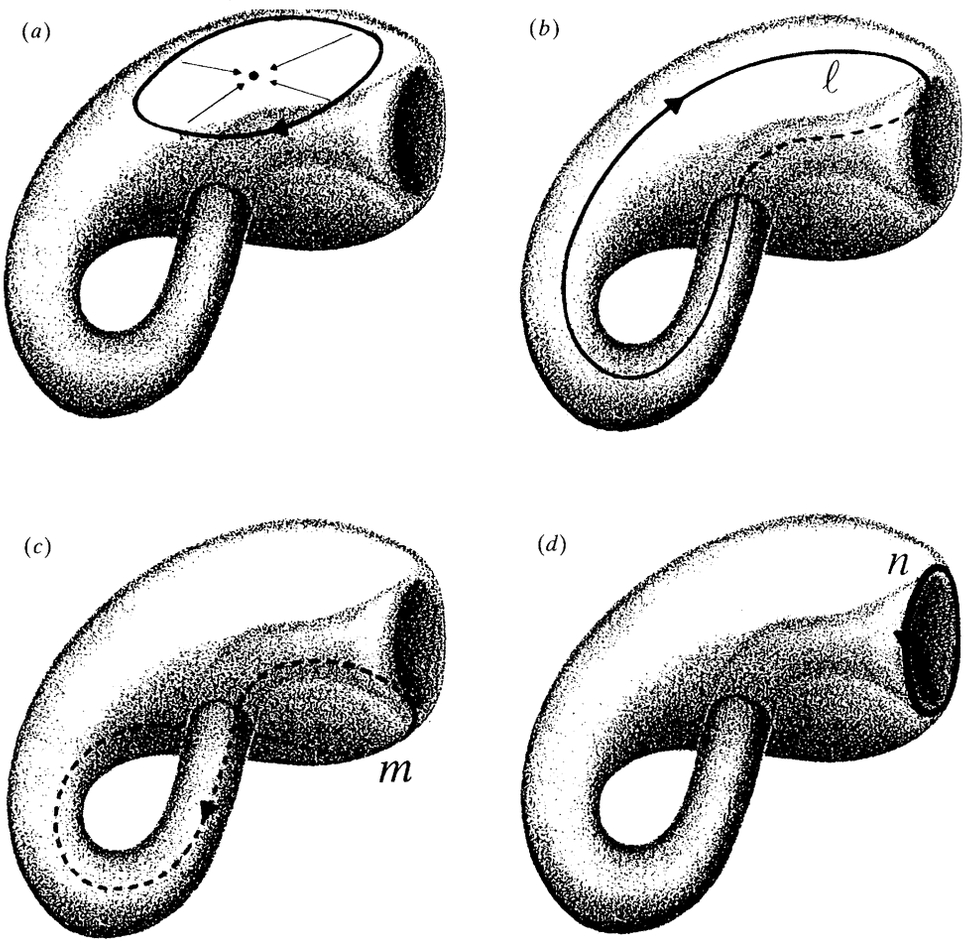

Figure 3. Loops on the Klein bottle. (*a*) A loop which can be reduced to a point by continuous deformation of the loop. In the topological theory on which all analyses in this research are based, loops can be freely deformed as if they are made of rubber. (*b*) A loop *l* surrounding the Klein bottle winding once along the top surface of the bottle specified by $\phi = 0°$. (*c*) A loop *m* surrounding the bottle winding once along the bottom surface of the bottle specified by $\phi = 180°$. (*d*) A loop *n* surrounding the bottle winding once around the bottle axis specified by $\theta = 0°$.

counterclockwise along the axis of the Klein bottle. A loop belonging to the homotopy class specified by $(0, 0)$ can be reduced by continuous deformation to a point (see figure 3*a*). However, a loop specified by $(p, q) \neq (0, 0)$ cannot be reduced to a point. The values of (p, q) for the loops shown in figure 3*b–d* are $(1, 0)$, $(1, 1)$ and $(0, 1)$, respectively. Homotopic loops of $(1, 0)$ and $(1, 1)$ can be mutually transformed by multiplying a homotopic loop of $(0, 1)$. Therefore, a loop over one side of the Klein bottle (*l* in figure 3*b*) is not homotopic to a loop over the other side (*m* in figure 3*c*). The homotopic loop of $(0, 1)$, *n* shown in figure 3*d* cannot be distinguished from a loop of the opposite direction, as these two can be mutually transformed by one round trip of the loops along the Klein bottle axis.

4. LOOP MAPPING

Now we assume that the optimal stimulus parameters are almost continuously represented over the cortical surface. This assumption is partly justified by the fact that the orientation changes continuously along the cortex except at isolated points, i.e. the orientation centres (see figure 1). When we move along a given loop on the cortical surface, the corresponding trajectory of the orientation and phase should form a loop on the Klein bottle because of the assumption of continuity in the orientation and phase. Let us identify two given point singularities in optimal stimulus parameters as elements of the same class of singularity, when the stimulus parameters around one point can be changed to those around the other by continuous transformation in the stimulus space. Because the continuous transformation in the stimulus space is equivalent to the continuous deformation of a loop on the Klein bottle, we can categorize point singularities through the categorization of loops on the Klein bottle according to whether they are transformed into one another by continuous loop deformation.

If the optimal stimulus parameters of neurons located along the circular loop on the cortical surface form the loops on the Klein bottle shown in figure 3, the configurations shown in figure 4 of RFS specified by the stimulus parameters are obtained. When a loop on the Klein bottle can be reduced to a point (see figure 3*a*), there are no singularities inside the cortical loop, as shown in figure 4*a*. However, when loops on the Klein bottle cannot be reduced to points (see figure 3*b–d*), the cortical loops contain point singularities (see figure 4b_1–*d*). Figure 4b_1, b_2 corresponds to figure 3*b*, but b_1 and b_2 have different directions of rotations in optimal orientation. Figure 4c_1, c_2 likewise corresponds

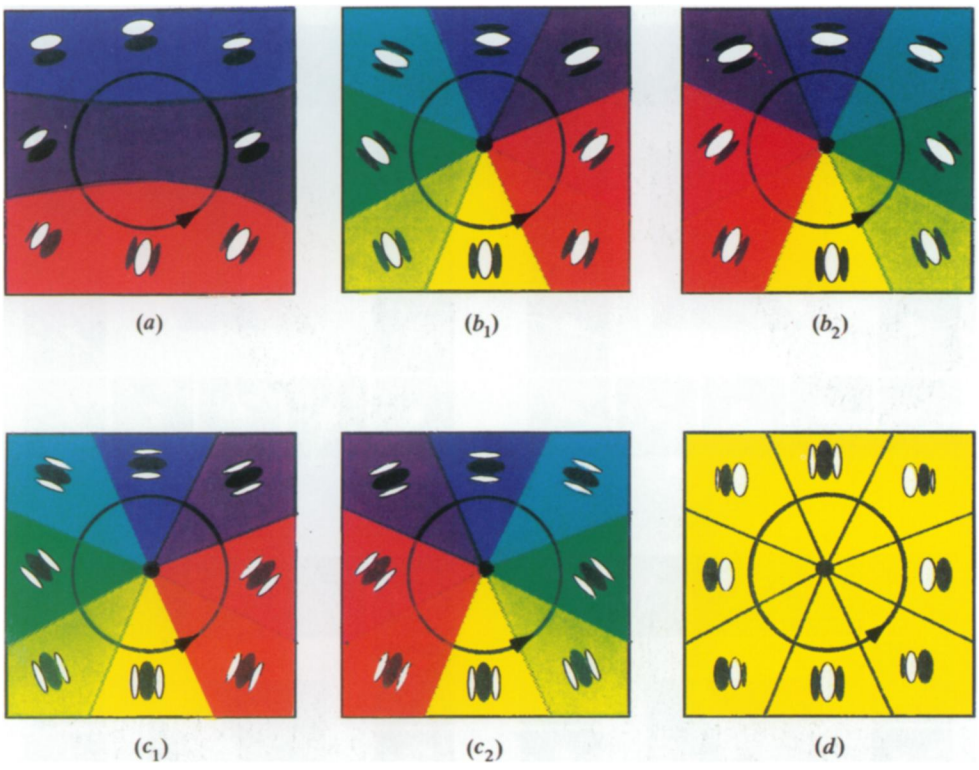

Figure 4. Possible configurations of RF profiles and local maps of optimal stimulus parameters. The optimal orientations are indicated by the colours. Point singularities indicated by the dots are contained in (*b*)–(*c*) but not in (*a*). (*a*) The net changes in orientation and phase amount to zero for one round trip along the cortical loop indicated by the circle, in the case where the corresponding loop on the Klein bottle (see figure 3*a*) can be reduced to a point. Note that orientation arrangements inside the dotted square in figure 1 are an actual example of this situation. (b_1), (b_2) When we move counterclockwise along the cortical loop, the orientation changes clockwise (b_2) or counterclockwise (b_1) by 180°, as correlated with the winding direction along the corresponding loop *l* on the Klein bottle (see figure 3*b*). (c_1), (c_2) Likewise, the orientation changes clockwise (c_2) or counterclockwise (c_1) by 180°, as correlated with the winding direction along the corresponding loop *m* (see figure 3*c*). Compare these orientation arrangements with pinwheel structures inside the two solid squares in figure 1. (*d*) When we move along the cortical loop *n* (see figure 3*d*), only the phase changes by 360°, with the orientation remaining unchanged.

to figure 3*c*. Interestingly, RFs around the point singularities in figure 4*b*, *c* are of ON-centre OFF-flank (in figure 4*b*) and OFF-centre ON-flank types (in figure 4*c*). Figure 4*d* shows another RF configuration corresponding to a loop around the Klein bottle axis shown in figure 3*d*.

5. COMPARISONS WITH SIMULATED RESULTS

We have developed a thermodynamic model for the self-organization of geniculo-cortical afferent inputs to reproduce simple-cell-like RFs and orientation preference maps (Miyashita & Tanaka 1992). Computer simulation based on this model (see Appendix) demonstrated the appearance of the four classes of orientation centres and one class of phase centres (point singularities about the phase) shown in figure 5. Here the optimal orientations of individual model cells were obtained as the directions of wave vectors averaged with the square of Fourier components as weights. The optimal phase values were extracted by the least-mean-square fitting of the simulated RFs to the Gabor functions with thus obtained orientations. Even though simulated RFs in the vicinity of orientation centres are slightly dissimilar to RFs derived from the Gabor function, clockwise or counterclockwise rotation in optimal orientation and ON-centre OFF-flank or OFF-centre ON-flank types of RFs can be clearly observed.

However, other types of point singularities such as $180°p$ ($p \geqslant 2$) could not be observed in the simulated orientation preference map. Generally, the creation of point singularities requires some additional energy as the RF abruptly changes in the vicinity of the points. It is expected that larger the value of p, greater the required energy. Thus the emergence of orientation centres of large p is prohibited energetically even if it is allowed topologically.

6. DISCUSSION

In comparison with the actual orientation preference map, the situation in figure 4*a* is the same as that inside the dotted square in figure 1. The RF configurations shown in figure 4*b*, *c* indicate the pinwheel-like structures inside the solid squares in figure 1, although the pinwheels of ON-centre OFF-flank and OFF-centre ON-flank types cannot be distinguished in the orientation preference map. From computational

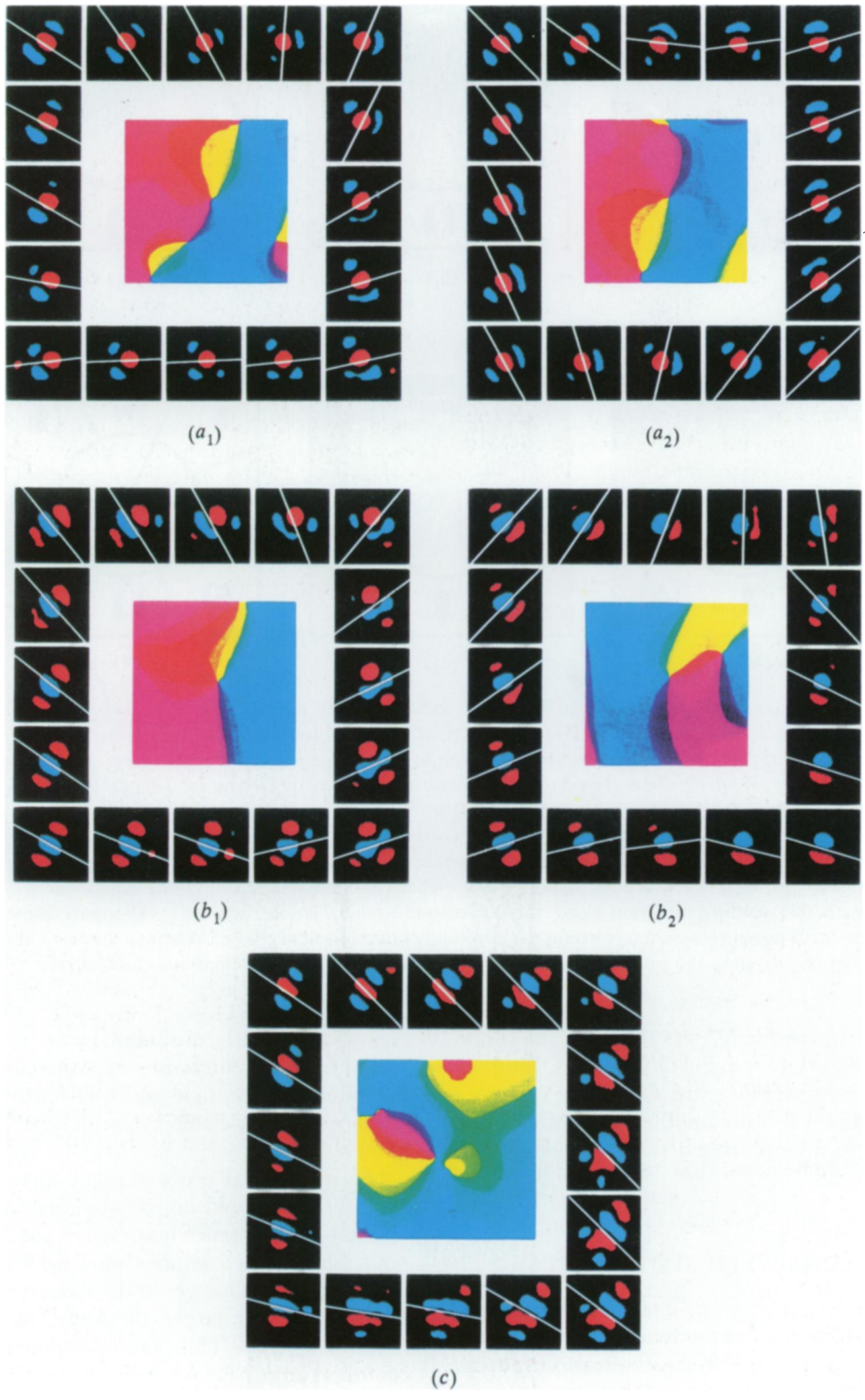

Figure 5. Configurations of simulated RF profiles and local maps of optimal stimulus parameters. The optimal orientations and phases are indicated by the colours. ON and OFF subfields of representative model neurons around the point singularities are indicated by red and blue. The white bars representing axes of the optimal orientations pass through the centres of individual RFs. Therefore, arrangements of ON and OFF subfields relative to the positions of the bars reflect phase values of the individual cells. Point singularities are shown in the centres of individual pictures as points around which all colours converge. Around the singularities about the optimal orientation shown in (a_1) and (a_2), all RFs were ON-centre OFF-flank types, and the orientation changed clockwise (a_2) or counterclockwise (a_1) by 180°. These configurations correspond to those shown in figure 4b_1, b_2, respectively. Around the singularities about the orientation shown in (b_1) and (b_2), all RFs were OFF-centre ON-flank types, and the orientation changes clockwise (b_2) or counterclockwise (b_1). These configurations correspond to those shown in figure 4c_1, c_2, respectively. There were point singularities around which the optimal phase changed by 360°, with the orientation remaining almost unchanged. A typical example obtained from the simulation shown in (c) corresponds to the RF configuration shown in figure 4*d*.

considerations regarding the contrast detection in stimulus luminance, these two types are required for a complete set of visual information representations. Therefore, it is suggested that these types of orientation centres may appear as pairs within one hypercolumn. Figure 4*d* shows that the phase changes by 360° around the phase centre whereas the orientation remains constant. This indicates that the phase centres can exist in iso-orientation domains.

Generally, if a loop winds p times around the Klein bottle along its axis, it will give rise to an orientation centre around which the change in orientation amounts to $180°p$. However, actual maps in the primary visual cortex have never been reported to contain orientation centres of 360° or more (Blasdel & Salama 1986; Bonhoeffer & Grinvald 1991). This may be explained by the conjecture that the energy required to create point singularities increases with p.

It has been reported that a single electrode sometimes recorded simultaneously activities from two adjacent cells of the cat visual cortex, whose phase values differ by 180° (Liu *et al.* 1992). This may suggest that the phase is not arranged in the cortex in a continuous manner. This study, however, shows that the phase can change drastically in the vicinity of the phase centres. Therefore, the experimental data cannot rule out the assumption of continuous mapping of the phase. Furthermore, all phases are represented around the phase centres with similar optimal orientations as shown in figures 4*c* and 5*c*. Therefore, it is expected that neurons which receive direct inputs from those cells do not exhibit phase dependence, as complex cells do not. This implies that phase centres have advantages for the formation of complex cells.

Even if we ignore the degree of freedom of the phase, orientation centres of the 180° version can be predicted when the optimal orientation is assumed to be invariant under 180° rotation in the stimulus space, as in most of the models for orientation column formation (Linsker 1985; Durbin & Mitchison 1990; Obermayer *et al.* 1990). This may be true for optimal orientations of complex cells whose RFs do not exhibit phase dependence. It should be noted that the emergence of the twisted structure of the stimulus space as the Klein bottle is attributed to the hidden symmetry inherent in the simple-cell RF which involves the phase as a relevant parameter. The same results cannot be derived from a naive assumption of the *a priori* existence of a cylindrical stimulus parameter space. Therefore, we may conclude that the involvement of simple cells in the map formation leads to the subdivision of orientation centres and the emergence of phase centres.

There are other degrees of freedom of stimulus parameters whose effects I did not examine here, such as spatial frequency, retinotopic position and ocular dominance. The coordinate axis of the spatial frequency is set in the thickness direction of the Klein bottle, and retinotopic distortion is thought to be small in the vicinity of orientation centres. These facts indicate that even if these parameters are incorporated in the analysis, the Klein bottle topology is preserved. Because in normal animals RFs in both eyes are similar (Hubel & Wiesel 1962), the trajectory of the optimal orientation and phase on the Klein bottle is continuous even across the border of ocular dominance columns. Therefore this topological approach remains valid.

Mathematics similar to those developed here may be applicable to the RF properties of other types of cells in the primary visual cortex and cells in other cortical areas. For instance, this topology-based approach can be extended to explain the spatial relations between orientation centres and singularities with respect to the optimal direction of motion (Swindale *et al.* 1987). I believe that this topological viewpoint will provide novel mathematical insights and lead to the understanding of mechanisms of cortical information representation.

I thank Professor Masao Ito and Dr Raymond T. Kado, for their continuous encouragement and critical readings of the manuscript. I acknowledge the kindness of Professor Amiram Grinvald in allowing me to use an unpublished photograph of the iso-orientation domains of cat area 17. Also I would like to thank Professor Horace Barlow and Professor Graeme Mitchison of the University of Cambridge for their important comments and suggestions for improving this manuscript.

APPENDIX

A model of self-organization and methods of computer simulation

In formulating the RF which describes neuronal responses to visual stimuli, I adopted a linear response framework. In this framework, the RF is defined as the fluctuation of neuronal activity in response to fluctuations in stimulus intensity:

$$R^{\mathrm{VC}}_{j,m} = \sum_{j'} \sum_{\mu} \sum_{k'} V^{\mathrm{post}}_{j;j'} \sigma_{j',k',\mu} \mu R^{\mathrm{G}}_{k';m}. \qquad \text{(A 1)}$$

Subscripts j and k indicate the position of afferent synaptic terminals and the position of presynaptic cell bodies, respectively. Subscript μ represents the centre type of presynaptic cells. When the presynaptic cell is of the ON-centre type, $\mu = +1$, and otherwise, $\mu = -1$. Equation (A 1) implies that the fluctuations in stimulus are propagated through the afferent inputs $\sigma_{j',k',\mu}$ and then summed by the synaptic interactions function $V^{\mathrm{post}}_{j;j'}$ determined by lateral connections to produce membrane polarization at a cortical neuron.

In the computer simulation, I adopted the Hamiltonian H which completely determines the behaviour of the system,

$$H = -\sum_{j,j'} \sum_{\substack{k \in B_j,\mu \\ k' \in B_{j'},\mu'}} V^{\mathrm{post}}_{j;j'} \Gamma^{\mathrm{pre}}_{k,\mu;k',\mu'} \sigma_{j,k,\mu} \sigma_{j',k',\mu'} + c/2 \sum_{k,\mu} (\sum_{j} \sigma_{j,k,\mu} - \bar{n})^2. \qquad \text{(A 2)}$$

The first term on the right-hand side is given by the synaptic interaction function $V^{\mathrm{post}}_{j;j'}$, the presynaptic correlation function of firings between a pair of neurons $\Gamma^{\mathrm{pre}}_{k,\mu,;k',\mu'}$ and the distribution of afferent inputs $\{\sigma_{j,k,\mu}\}$.

The set of presynaptic neurons which can form synaptic connections at position j in the postsynaptic layer are given by B_j. The probability of existence of terminals of afferent inputs from the presynaptic neuron at position k to synaptic position j is assumed to depend on the distance $d_{k;K_j}$ between k and the topographically corresponding position K_j. This probability is given by

$$P_{k;j} = \exp\left[-d^2_{k;K_j}/(2\lambda^2_{\mathrm{Arb}})\right], \qquad \text{(A 3)}$$

where λ_{Arb} determines the extent of possible afferent arborization.

The second term on the right-hand side of equation (A 2) imposes a restriction so that the number of synaptic terminals of a presynaptic neuron, $n_{k,\mu} = \sum_j \sigma_{j,k,\mu}$, tends to the average number $\bar{n}$.

The spatial dependence of the function representing the synaptic interaction, which was maintained unchanged during self-organization, was assumed to be short-range excitatory and long-range inhibitory. It is given by a difference of Gaussian functions:

$$V^{\mathrm{post}}_{j;j'} = [q_{\mathrm{ex}}/(2\pi\lambda^2_{\mathrm{ex}})] \exp(-d^2_{j;j'}/2\lambda^2_{\mathrm{ex}}) - [q_{\mathrm{inh}}/(2\pi\lambda^2_{\mathrm{inh}})] \exp(d^2_{j;j'}/2\lambda^2_{\mathrm{inh}}). \quad (A\ 4)$$

Parameters q_{ex} and q_{inh} represent excitatory and inhibitory interaction strengths, which are given by the integration of each part of the function with respect to position j'. Parameters λ_{ex} and λ_{inh} represent excitatory and inhibitory interaction lengths.

The presynaptic correlation function $\Gamma^{\mathrm{pre}}_{k,\mu;k',\mu'}$ describes the correlation in activity between two neurons in the lateral geniculate nucleus (LGN) which corresponds to the presynaptic layer. For simplicity, if we assume that the LGN serves only as a relay nucleus and does not contribute any additional information processing, the presynaptic correlation function can be looked upon as that in the layer of retinal ganglion cells. Thus we must discuss the correlation properties of the retinal ganglion cells.

It is assumed that the value of the correlation function should be positive between same centre-type retinal ganglion cells and negative between the opposite centre-type cells (Miyashita & Tanaka 1992). This produces the competition between ON- and OFF-centre afferent inputs, in the result that ON and OFF subfields are segregated within individual RFs. The spatial profile of the correlation function is given by the convolution of RFs of two retinal ganglion cells. The ON-centre type RF of a retinal ganglion cell $R^{\mathrm{G}}_{k;m}$ is given by the function

$$R^{\mathrm{G}}_{k;m} = [q_{\mathrm{c}}/(2\pi\lambda^2_{\mathrm{c}})] \exp(-d^2_{k;m}/2\lambda^2_{\mathrm{c}}) - [q_{\mathrm{p}}/(2\pi\lambda^2_{\mathrm{p}})] \exp(-d^2_{k;m}/2\lambda^2_{\mathrm{p}}), \quad (A\ 5)$$

where the parameters q_{c} and q_{p} represent the strengths of the centre and periphery of the RF, respectively, and λ_{c} and λ_{p} represent the corresponding lengths.

The visual cortex is modelled by a square plane of 100×100 pixels. The LGN is modelled as two square planes of 20×20 neurons, which represent neuronal layers composed of ON- and OFF-centre cells.

First, a synaptic connection pattern is prepared as a regular topographic projection from the LGN to the visual cortex. The initial pattern of synaptic connections for Monte Carlo computer simulations are obtained by 1×10^5 random exchanges of the positions of randomly selected pairs of adjacent synaptic terminals. In these random exchanges, each synaptic terminal diffuses within the extent allowed by the probability given by equation (A 3).

The main part of the simulation conforms to the Monte Carlo technique in which a synaptic terminal at a randomly selected position is replaced with another terminal according to the value of the probability. The probability is determined by the energy difference between the states before and after the replacement, as follows:

$$\mathrm{Prob}(\mathrm{before} \rightarrow \mathrm{after}) = 1/\{1 + \exp[\beta(E^{\mathrm{after}} - E^{\mathrm{before}})]\}. \quad (A\ 6)$$

One Monte Carlo step is defined as 100×100 repetitions of trials of the synaptic terminal replacements. The system reached equilibrium after 500 Monte Carlo steps, at which the energy takes a constant value, the Monte Carlo simulation ceased.

The values of parameters used in the simulation are as follows: $q_{\mathrm{ex}} = 1.0$, $q_{\mathrm{inh}} = 0.6$, $\lambda_{\mathrm{ex}} = 0.75$, $\lambda_{\mathrm{inh}} = 1.5$, $q_{\mathrm{c}} = 1.0$, $q_{\mathrm{p}} = 0.8$, $\lambda_{\mathrm{c}} = 0.4$, $\lambda_{\mathrm{p}} = 1.0$, $\lambda_{\mathrm{Arb}} = 2.0$, $\bar{n} = 15$ and $\beta = 1000$. The value of the coefficient c in the restriction term was chosen so that the average value of the restriction was one-quarter of the average value of the energy difference during simulation.

REFERENCES

Blasdel, G. G. 1992 Orientation selectivity, preference, and continuity in monkey striate cortex. *J. Neurosci.* **12**, 3139–3161.

Blasdel, G. G. & Salama, G. 1986 Voltage-sensitive dyes reveal a modular organization in monkey striate cortex. *Nature, Lond.* **321**, 579–585.

Bonhoeffer, T. & Grinvald, A. 1991 Iso-orientation domains in cat visual cortex are arranged in pinwheel-like patterns. *Nature, Lond.* **353**, 429–431.

Bredon, G. E. 1993 *Topology and geometry, Graduate texts in mathematics*, p. 139. New York: Springer-Verlag.

Daugman, J. G. 1980 Two-dimensional spectral analysis of cortical receptive field profiles. *Vis. Res.* **20**, 847–856.

Durbin, R. & Mitchison, G. 1990 A dimension reduction framework for understanding cortical maps. *Nature, Lond.* **343**, 644–647.

Hubel, D. H. & Wiesel, T. N. 1962 Receptive fields, binocular interaction and functional architecture in the cat's visual cortex. *J. Physiol.* **160**, 106–154.

Linsker, R. 1986 From basic network principles to neural architecture: Emergence of orientation columns. *Proc. natn. Acad. Sci. U.S.A.* **83**, 8779–8783.

Liu, Z., Gaska, J. P., Jacobson, L. D. & Pollen, D. A. 1992 Interneuronal interaction between members of quadrature phase and anti-phase pairs in the cat's visual cortex. *Vis. Res.* **32**, 1193–1198.

Marcelja, S. 1980 Mathematical description of the responses of simple cortical cells. *J. opt. Soc. Am.* **70**, 1297–1300.

Miller, K. D. 1992 Development of orientation columns via competition between on- and off-center inputs. *NeuroReport* **3**, 73–76.

Miyashita, M. & Tanaka, S. 1992 A mathematical model for the self-organization of orientation columns in visual cortex. *NeuroReport* **3**, 69–72.

Obermayer, K., Ritter, H. & Schulten, K. 1990 A principle for the formation of the spatial structure of cortical maps. *Proc. natn. Acad. Sci. U.S.A.* **87**, 8345–8349.

Swindale, N. V., Matsubara, J. A. & Cynader, M. S. 1987 Surface organization of orientation and direction selectivity in cat area 18. *J. Neurosci.* **7**, 1414–1427.

von der Malsburg, C. 1973 Self-organization of orientation selective cells in the striate cortex. *Kybernetik* **14**, 85–100.

Received 6 February 1995; accepted 21 March 1995